Wind farm performance in conventionally neutral atmospheric boundary layers with varying inversion strengths

2014 J. Phys.: Conf. Ser. 524 012114

(http://iopscience.iop.org/1742-6596/524/1/012114)

Wind farm performance in conventionally neutral atmospheric boundary layers with varying inversion strengths

Dries Allaerts and Johan Meyers

Department of Mechanical Engineering, Celestijnenlaan 300 box 2421, BE 3001 Leuven (Heverlee), Belgium

E-mail: dries.allaerts@kuleuven.be

Abstract. In this study we consider large wind farms in a conventionally neutral atmospheric boundary layer. In large wind farms the energy extracted by the turbines is dominated by downward vertical turbulent transport of kinetic energy from the airflow above the farm. However, atmospheric boundary layers are almost always capped by an inversion layer which slows down the entrainment rate and counteracts boundary layer growth. In a suite of large eddy simulations the effect of the strength of the capping inversion on the boundary layer and on the performance of a large wind farm is investigated. For simulations with and without wind turbines the results indicate that the boundary layer growth is effectively limited by the capping inversion and that the entrainment rate depends strongly on the inversion strength. The power output of wind farms is shown to decrease for increasing inversions.

1. Introduction

Traditionally, atmospheric boundary layers (ABLs) are categorized as neutral, stable or unstable based on the heat flux at the earth's surface. Over the last decade, however, several studies have revealed that the background stratification, against which the boundary layer is developing, greatly influences all properties of the ABL and that it should be included in the classification of atmospheric flows. For neutral ABLs, Zilitinkevich and Esau [1] suggest distinguishing between truly neutral flows, developing in a neutrally stratified fluid, and conventionally neutral flows, developing against a stable stratification. Based on meteorological data, spanning a period of almost one century, Hess [2] has concluded that the truly neutral ABL is an idealised case that 'does not seem to exist in the atmosphere, or is so rare that it has not been well observed'. The conventionally neutral atmospheric boundary layer (CNBL) will be the subject of the present study.

Figure 1 shows schematic profiles of the potential temperature and the magnitude of the velocity in a CNBL. As indicated, a very stable, thin layer can often be found between the neutral boundary layer and the stable free atmosphere aloft. This so-called capping inversion is characterized by its thickness, the temperature difference across the layer (the inversion strength), and the height of the inversion base. Inside the capping inversion, large negative buoyancy forces decelerate the turbulent gusts that try to penetrate into the free atmosphere. As a result, the turbulent entrainment process at the top of the boundary layer is slowed down and further deepening of the boundary layer is prevented. These forces originate from the

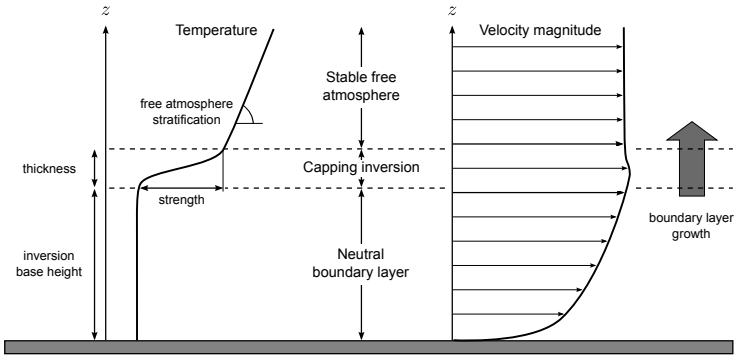

Figure 1. Schematic view of the conventionally neutral atmospheric boundary layer, showing profiles of the potential temperature and the magnitude of the velocity as a function of height.

potential temperature gradient, suggesting that, for a given thickness, the inversion strength could be a key parameter in the boundary layer scaling. This argument is not supported in the existing literature on CNBLs, where all proposed parametrizations of the ABL height are only based on the free atmosphere stratification. However, we do find support for our reasoning in literature on entrainment parametrizations in convective boundary layers. Already in 1968, Lilly [3] predicted that for convective boundary layers the rate of rise of the inversion base is inversely proportional to the inversion strength, and many others followed with more advanced correlations [4–6].

Since the realization that an important difference exist between the truly and conventionally neutral atmospheric boundary layer, various studies have been dedicated to this atmospheric flow type [2, 7–9]. In these studies, large eddy simulations are typically initialized with a linearly increasing potential temperature of which the gradient is equal to the free atmosphere lapse rate. After a certain simulation time, quasi-steady state can be achieved and the resulting boundary layer height is dependent on the free atmosphere stratification. However, no justification is given for the rather arbitrarily chosen initial linear potential temperature profile. Based on a zero-order model analysis of the entrainment caused by CNBLs, Tennekes [4] showed that the evolution of the CNBL is so slow that it critically depends on the initial condition. He also concluded that the lapse rate above the ABL plays no role when the initial inversion base height or the initial inversion strength is very large. This conclusion is in sharp contradiction with the use of the free atmosphere stratification as a key scaling parameter. In the present study we will investigate the influence of varying inversion strengths on the underlying neutral boundary layer while carefully selecting the initial conditions.

A second research question that this study addresses is to which extent the capping inversion influences a large wind farm situated in the neutral boundary layer below. In large wind farms the energy extracted by the turbines is dominated by downward vertical turbulent transport of kinetic energy from the airflow above the farm [10]. Additionally, turbulence intensities increase because of the presence of the turbines. In contrast with the capping inversion, wind farms actually enhance the vertical entrainment of air into the farm and increase the boundary layer growth above the farm. It is to be expected that, depending on the height and strength of the inversion, that the CNBL will have an influence on the amount of energy that can be transported towards the turbines and hence the amount of power that the wind farms can extract.

The present paper has been organised in the following way. In section 2 the simulation code used in this study is introduced and the various cases are described. Results are given in section 3. The last section summarizes our conclusions.

2. Methodology

2.1. LES Governing Equations

The CNBL is modelled using large eddy simulations (LES). In order to allow simulations of the capping inversion and part of the free atmosphere above the boundary layer, the LES is based on the filtered transport equation for the potential temperature combined with the filtered Navier-Stokes equations and the filtered continuity equation, i.e.

$$\partial_i \tilde{u}_i = 0, \tag{1}$$

$$\partial_t \tilde{u}_i + \tilde{u}_j \partial_j \tilde{u}_i = \delta_{i3} g(\tilde{\theta} - \langle\tilde{\theta}\rangle)/\theta_0 + f_c \epsilon_{ij3} \tilde{u}_j - \partial_i \tilde{p}^\star - \partial_j \tau^r_{ij} + f_i, \tag{2}$$

$$\partial_t \tilde{\theta} + \tilde{u}_j \partial_j \tilde{\theta} = -\partial_j q_j, \tag{3}$$

where $\tilde{u}_i$ and $\tilde{\theta}$ are the filtered velocity and potential temperature fields, respectively, and the angular brackets denote horizontal averaging. Further, g is the gravitational acceleration, f_c is the Coriolis parameter and $\tilde{p}^\star = \tilde{p}'/\rho_0 + \tau_{kk}/3$ is the filtered modified pressure. Thermodynamic state variables describing the adiabatic, motionless, dry background state are denoted with subscript zero. The Boussinesq approximation implies that the background density ρ_0 and the potential temperature θ_0 are taken constant, and hydrostatic pressure variations with height are included in the background pressure $p_0(z)$ [11]. Primed variables such as $\tilde{p}'$ indicate deviations from the adiabatic background state. Molecular diffusion and viscosity terms are neglected since in most atmospheric flows these terms are several orders of magnitude smaller than any other term in the equations.

The subgrid-scale stress term and heat flux are defined as

$$\tau_{ij} = \widetilde{u_i u_j} - \tilde{u}_i \tilde{u}_j, \quad q_j = \widetilde{u_j \theta} - \tilde{u}_j \tilde{\theta} \tag{4}$$

and the trace of the stress term $\tau_{kk}/3$ is combined into the modified pressure. The deviatoric part of the stress term $\tau^r_{ij} = \tau_{ij} - \delta_{ij}\tau_{kk}/3$ is computed with an eddy-viscosity model. The heat flux is modelled with an eddy-diffusivity model using a constant prescribed turbulent Prandtl number. The eddy viscosity follows from a standard Smagorinsky model [12] where classic wall damping of the Smagorinsky length scale is applied near the bottom surface [13].

Simulations are performed with the in-house large eddy simulations code SP-Wind, which is an updated version of the KU Leuven code described by Calaf et al. [10]. In the code horizontal directions are discretised spectrally and use periodical boundary conditions. The vertical direction uses a fourth-order energy-conservative finite difference scheme [14]. At the top of the domain, a zero shear stress boundary condition is applied for the horizontal velocities and the vertical velocity is set to zero. The potential temperature at the upper boundary is held constant, assuming that the top of the domain is high enough not to be influenced by the boundary layer. Classic wall stress formulation based on the standard log (Monin-Obukhov) similarity law is used to model the drag exerted by the Earth's surface [15]. The CNBL is characterised by a zero surface heat flux, so no wall model is needed for the potential temperature equation. Finally, time integration of the velocity and temperature fields is performed using a classical four-stage fourth-order Runge-Kutta scheme and wind turbines are modelled using a non-rotating Actuator Disk Method (ADM).

2.2. Wind Angle Controller

The length scale of turbulent flow in the atmospheric boundary layer is so large that the Coriolis force caused by the rotation of the earth becomes an important term in the momentum balance. In this study the flow above the boundary layer is approximately steady, horizontal and homogeneous in horizontal planes, which means that the Coriolis force has to be balanced by the pressure gradient in the absence of turbulent shear stresses. As a result of this force balance,

the air must flow parallel to the pressure contours. Upon entering the boundary layer, shear stresses will start influencing the force balance and will result in a change in wind direction with respect to the flow above the boundary layer. In a truly neutral boundary layer this effect is well known and is called the Ekman spiral [16]. For conventionally neutral cases the magnitude of this effect is the result of a complex dynamical system, which makes it unpredictable and dependent on the characteristics of the capping inversion and the development of the flow field.

The wind direction at the hub height of the wind turbines is an uncontrolled result of the specified geostrophic angle. However, the wind direction should be perpendicular to the blades of the turbines since ADM modelling is used. One possible solution would be to allow the turbines to yaw in the simulations, but this would result in a continuously changing geometrical pattern of the wind farm. Instead, a method similar to the one proposed by Sescu and Meneveau [17] is followed where pseudo forces are included to gradually adjust the wind direction. However, instead of using an arbitrary angular velocity, the pseudo forces are considered as a result of the rotation of the reference frame around the vertical axis. The angular velocity of the reference frame should be chosen such that the rotation of the velocity vector at hub height is cancelled out. In this way the wind direction at the turbines is always aligned with the x-direction and a fixed wind farm geometry is assured.

The effective angular velocity consists of two terms. The first term depends on the rotation of the wind speed at hub height

$$\omega = \frac{\phi^n - \phi^{n-1}}{\Delta t}, \quad \tan\phi = \frac{\langle V(z_h)\rangle}{\langle U(z_h)\rangle} \tag{5}$$

where ϕ^n is the wind angle at hub height at timestep n. This rotation speed is filtered over time with time constant σ in order to average out turbulent fluctuations in the wind angle. The second term contributing to the angular velocity of the reference frame penalizes the error between the current angle at the hub height and the preferred angle. The effective angular velocity is a linear combination of both terms

$$\omega_e = \bar{\omega} + \beta(\phi - \phi_{ref}) \tag{6}$$

where $\bar{\omega}$ denotes the time filtered quantity.

2.3. Capping Inversion Quantification

The LES code produces three-dimensional velocity and potential temperature fields as output. Assuming horizontal homogeneity, averaged profiles in function of the vertical coordinate can be obtained from these three-dimensional fields. For post-processing purposes, however, precise estimates of quantities such as the inversion base height or the inversion strength are required (based on the potential temperature), but these quantities can not be read directly from vertical potential temperature profiles. In order to describe the vertical structure of the ABL in terms of a conceptual model based on general quantities, the approach of Rampanelli and Zardi [18] is followed. The method consist in a best-fit analysis with a predefined smooth test function

$$\theta(z) = \theta_m + a\frac{\tanh(\eta)+1}{2} + b\frac{\ln[2\cosh(\eta)]+\eta}{2}, \tag{7}$$

where $\eta = (z-l)/c\Delta h$ is the dimensionless vertical displacement from a reference height l and θ_m is the potential temperature of the underlying mixed-layer. The constants a, b and c can be related to the inversion strength $\Delta\theta$, the base, center and top of the inversion h_0, h_1 and h_2 and the free atmosphere stratification γ. Figure 2 shows the smooth test curve along with the definition of the physical quantities.

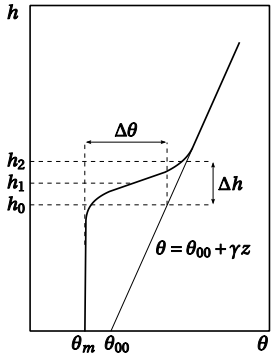

Figure 2. Smooth test curve for potential temperature profile fitting, indicating the physical variables defining the capping inversion. Figure adopted from Rampanelli and Zardi [18].

Table 1. Overview of the various LES cases with the initial inversion strengths $\Delta\theta_0$ and the number of wind turbines N_t.

	$\Delta\theta_0$ [K]	N_t
A1	2.5	—
A2	5	—
A3	10	—
B1	2.5	8×6
B2	5	8×6
B3	10	8×6

Once the mathematical parameters defining the curve have been solved for, the physical variables defining the capping inversion can be computed. This procedure will be applied to the instantaneous potential temperature profile at each post-processing step in order to allow detailed analysis of the evolution of the capping inversion.

2.4. Numerical Setup

The effect of the capping inversion on the atmospheric boundary layer and on the wind farm performance is investigated by running three simulations with different initial inversion strengths. The simulations are performed both with and without wind farms. Tabel 1 gives an overview of the various LES cases with the initial inversion strengths and the number of wind turbines. Barotropic atmospheric condition are assumed and the driving geostrophic wind speed is set equal to 10 m/s.

The velocity and potential temperature fields are initialized with appropriate vertical mean profiles and random perturbation are included in the lower 100 m of the velocity fields to trigger turbulence. The initial mean velocity profile is a combination of a constant velocity profile equal to the geostrophic wind above the initial capping inversion and a neutral boundary layer profile below. The lower initial velocity profile is defined by

$$u(z) = \frac{u_\tau}{\kappa}\left[\ln\frac{z}{z_0} + f_u(\zeta)\right], \quad v(z) = -\frac{u_\tau}{\kappa} f_v(\zeta)\,\mathrm{sign} f, \tag{8}$$

where f_u and f_v are universal functions of the non-dimensional height $\zeta = z/h_0$ [19], κ is the von Karman constant and u_τ is the friction velocity. The initial potential temperature profile is produced with equation (7) using the inversion strengths from table 1. The free atmosphere stratification is set to 1 K/km and the constant potential temperature of the boundary layer

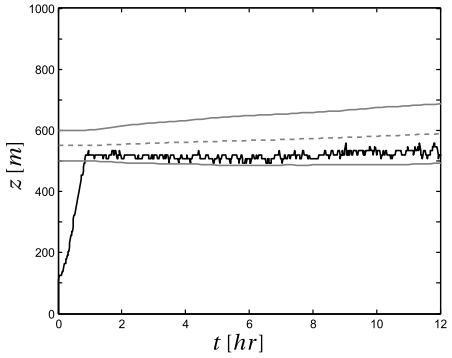

Figure 3. Time evolution of the boundary layer height h_M (solid black line), defined as the level at which the tangential turbulent stress vanishes, and the vertical structure of the capping inversion, including upper and lower limits h_2 and h_0 (solid grey lines) and center line h_1 (dashed grey line) for simulation A1.

$\theta_m = 288.15\,\mathrm{K}$, which is also chosen as the reference temperature θ_0. The initial inversion layer starts at $h_0 = 500\,\mathrm{m}$ and has a thickness $\Delta h = 100\,\mathrm{m}$. Further, the surface roughness z_0 and the surface Rossby number Ro are set to 0.1 m and 10^6, respectively, corresponding to land based atmospheric flow at a latitude $\phi = 43.43°$.

The height of the simulation domain L_z is set to 1 km and the horizontal size is set to $L_x \times L_y = (2\pi \times \pi)L_z$. The grid has a size of $128 \times 128 \times 80$ and is uniform in all directions. In the simulations with wind farm the wind turbines have a hub height $z_h = 100\,\mathrm{m}$ and diameter $D = 100\,\mathrm{m}$. The wind turbine grid is 8×6 and the spacing between the turbines relative to the diameter is given by $s_x = 7.854$ and $s_y = 5.236$. The numerical grid size for simulations with wind turbines is refined to $128 \times 256 \times 80$ in order to have similar y and z spacing. All simulations span a time period of 20 hours and instantaneous vertical profiles of the potential temperature are saved every 10 minutes.

3. Results

First the behaviour of the CNBL under varying inversion strengths in the absence of wind turbines is studied. Figure 3 shows the variation in time of the boundary layer height and the structure of the capping inversion for simulation A1. Following Kosovic and Curry [20], the height of the ABL can be estimated as the height at which the tangential turbulent stress vanishes. This height is computed as a linear extrapolation of the height where the tangential turbulent stress is reduced to 5% of its surface value:

$$h_M = \frac{z\left[\left(\langle u'w'\rangle^2 + \langle v'w'\rangle^2\right)^{0.5} = 0.05u_\tau^2\right]}{0.95} \tag{9}$$

This estimate is shown in Figure 3 as the solid black line. The base, center and top of the inversion can be obtained from the analysis of the vertical potential temperature profile, which are represented as grey lines in Figure 3. After a start-up phase of about one hour, the estimate of the boundary layer height based on the momentum equation coincides with the inversion base. This result proves that the capping inversion acts as a rigid lid on the boundary layer and counteracts further growth. Further, it can be observed that turbulence manages to penetrate into the lower part of the inversion layer and that the estimate of the height of the boundary layer based on the turbulent stresses lies above the inversion base. In addition, the boundary layer is allowed to grow in time at a slow pace.

A more detailed view of the capping inversion structure for varying inversion strengths is shown in Figure 4. Here it appears that for increasing inversion strengths the repression of turbulence in the capping inversion is stronger and the height of the boundary layer is more strictly confined to the inversion base. Boundary layer growth is almost completely suppressed in simulations A2 and A3. From the time evolution of the top of the inversion it appears that

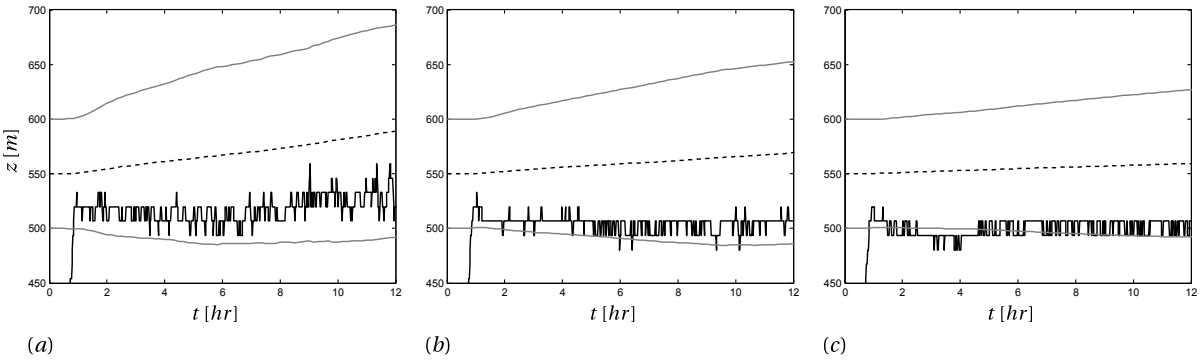

Figure 4. Detailed view of the time evolution of the boundary layer height h_M (solid black line), defined as the level at which the tangential turbulent stress vanishes, and the vertical structure of the capping inversion, including upper and lower limits h_2 and h_0 (solid grey lines) and center line h_1 (dashed grey line) for simulations A1 (a), A2 (b) and A3 (c) without wind turbines.

Table 2. Integral measures of the CNBL for the LES cases without wind turbines.

	α [°]	C_g [−]	$\int_0^{h_0} \epsilon \, \mathrm{d}z$ [Wm/kg]	$\mathrm{d}h_0/\mathrm{d}t$ [m/hr]
A1	-24.3717 [100.00 %]	0.0427 [100.00 %]	1.6609 [100.00 %]	2.9605 [100.00 %]
A2	-25.0398 [102.74 %]	0.0425 [99.53 %]	1.6381 [98.63 %]	1.9166 [64.74 %]
A3	-25.4944 [104.61 %]	0.0424 [99.30 %]	1.6254 [97.86 %]	0.7212 [24.36 %]

capping inversions with higher inversion strengths form a more coherent structure that is less prone to turbulent mixing and can better preserve its shape.

Table 2 compares frequently used integral measures of the CNBL for the simulations without wind turbines. The values are averaged over the last hour of the simulation. For increasing inversion strength the geostrophic angle α, defined as the angle between the direction of the wind in the free atmosphere and the direction of the shear stress at the surface, increases with almost 5 percent from simulation A1 to A3. In the geostrophic drag $C_g = u_\tau / G$ no significant decrease can be observed. The mean flow kinetic energy dissipation integrated over the depth of the boundary layer can be computed as [19]

$$\int_0^{h_0} \epsilon \, \mathrm{d}z = G u_\tau^2 \cos\alpha \tag{10}$$

and decreases a few percent for inversion strengths going form 2.5 K tot 10 K. The most striking result to emerge from the data is that the entrainment rate $\mathrm{d}h_0/\mathrm{d}t$, obtained from the potential temperature profile analysis, shows a substantial decrease of more than 75 % for increasing inversion strength.

Figure 5 illustrates what happens when a wind farm is inserted into the CNBL. Interestingly, the addition of a wind farm strongly increases the turbulent intensity of the boundary layer and yields a much more chaotic behaviour of the boundary layer height. Moreover, the entrainment rate in the cases with wind farms is much bigger than those without wind farms. Nevertheless, the CNBL height is just as before bounded by the capping inversion and the growth rate is determined by the strength of the inversion, being smaller for higher strengths. Finally it

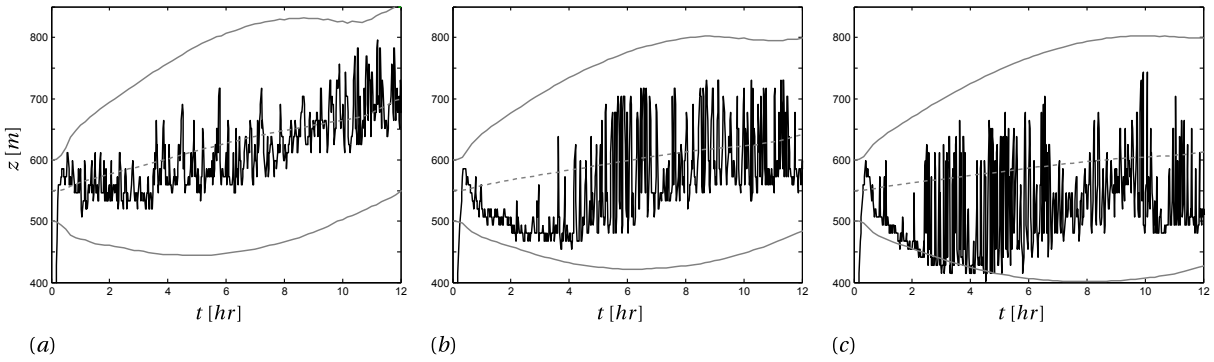

Figure 5. Detailed view of the time evolution of the boundary layer height h_M (solid black line), defined as the level at which the tangential turbulent stress vanishes, and the vertical structure of the capping inversion, including upper and lower limits h_2 and h_0 (solid grey lines) and center line h_1 (dashed grey line) for simulations B1 (a), B2 (b) and B3 (c) with wind turbines.

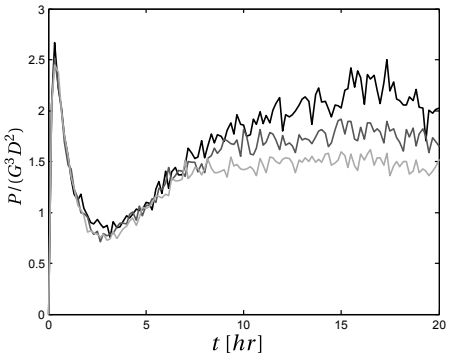

Figure 6. Non-dimensional wind farm power output as a function of time for simulations B1 (black line), B2 (dark grey line) and B3 (light grey line).

appears that turbulent gusts manage to penetrate farther into the inversion layer so that the height of the boundary layer coincides with the center rather than with the base of the inversion.

The performance of the wind farms in the different simulations is compared in Figure 6. The results show a rather long initialization period of about 5 hours. After this transitional phase, the power output appears to be larger for wind farms situated in a boundary layer capped by a weak inversion. This important effect is related to the vertical transport of energy from above the farm towards the turbines. For stronger inversions, the amount of energy that can be entrained from the air above the farm is restricted more severely. The power of the wind farm in simulation B1 turns out to be more than 30 % higher than the power output in simulation B3 after the initialization period.

4. Conclusion

The purpose of the current study was to determine the effect of the capping inversion on the conventionally neutral atmospheric boundary layer and on the performance of a wind farm. In the CNBL the very stable inversion layer weakens the turbulent entrainment process at the top of the boundary layer and limits the growth of the ABL. For these reasons it was anticipated that the inversion strength would form a key parameter in the boundary layer structure. In a suite of LES simulations without wind farms it was shown that the neutral boundary layer is effectively limited in growth by the capping inversion and that the resulting entrainment rates are dependent on the strength of the inversion. However, other frequently used integral measures of the boundary layer showed small to no dependence on the inversion strength.

When including a wind farm in the simulations, the same trends were observed as for the simulations without turbines, i.e. the growth of the fully developed wind turbine array boundary layer is slowed down by the capping inversion, and the size of the effect depends on the strength. As expected, the performance of the wind farm was also influenced by the inversion layer. A capping inversion with a strength of 2.5 K causes a difference in the power output of the turbines of more than 30 % with respect to a strong inversion of 10 K.

The results of this study show that the capping inversion can have a considerable impact on the atmospheric boundary layer, and also impacts on power extraction of wind-farms in the ABL. In the current study, we only investigated the effect of varying inversion strengths. We believe that for the determination of the wind-farm energy yield the height of the inversion base is also important, in particular when this height is only a few times the turbine height, as may be encountered in off-shore situations. This is currently a topic of further research.

Acknowledgments
The authors acknowledge support from the European Research Council (FP7–Ideas, grant no. 306471). Simulations were performed on the computing infrastructure of the VSC Flemish Supercomputer Center, funded by the Hercules Foundation and the Flemish Government.

References

[1] Zilitinkevich S S and Esau I N 2002 *Boundary-Layer Meteorol.* **104** 371–379
[2] Hess G D 2004 *Boundary-Layer Meteorol.* **110** 319–355
[3] Lilly D K 1968 *Q. J. R. Meteorol. Soc.* **94** 292–309
[4] Tennekes H 1973 *J. Atmos. Sci.* **30** 558–567
[5] Deardorff J W 1979 *J. Atmos. Sci.* **36** 424–436
[6] VanZanten M C, Duynkerke P G and Cuijpers J W M 1999 *J. Atmos. Sci.* **56** 813–828
[7] Esau I N 2004 *Ann. Geophys.* **22** 3353–3362
[8] Taylor J R and Sarkar S 2008 *Int. J. Heat Fluid Flow* **29** 721–732
[9] Abkar M and Porté-Agel F 2013 *Energies* **6** 2338–2361
[10] Calaf M, Meneveau C and Meyers J 2010 *Phys. Fluids* **22**(015110)
[11] Wyngaard J C 2010 *Turbulence in the Atmosphere* (New York: Cambridge University Press)
[12] Smagorinsky J 1963 *Mon. Weather Rev.* **91** 99
[13] Mason P J and Thomson D J 1992 *J. Fluid Mech.* **242** 51–78
[14] Verstappen R W C P and Veldman A E P 2003 *J. Comput. Phys.* **187** 343–368
[15] Moeng C H 1984 *J. Atmos. Sci.* **41** 2052–2062
[16] Tennekes H and Lumley J L 1972 *A first course in turbulence* (MIT press)
[17] Sescu A and Meneveau C 2014 *Q. J. R. Meteorol Soc.* (*Preprint* `10.1002/qj.2266`)
[18] Rampanelli G and Zardi D 2004 *J. Appl. Meteor.* **43** 925–933
[19] Zilitinkevich S S 1989 *Boundary-Layer Meteorol.* **46** 367–387
[20] Kosovic B and Curry J 2000 *J. Atmos. Sci.* **57** 1052–1068